Cardiology Plus

OPEN

Histological validation of artificial intelligence–driven automatic plaque characterization in coronary OCT: a head-to-head comparison with clinicians

Miao Chu[1,2], Francesca Razzi[3], Giovanni Luigi De Maria[2], Stefano Benenati[2,4], Jason Chai[2], Wei Yu[1], Ruobing Dai[1], Volkert van Steijn[5], Adrian Banning[2], Juan Luis Gutiérrez-Chico[6], Shengxian Tu[1,2]*, Heleen van Beusekom[3]

Abstract

Background and purpose: Artificial intelligence (AI) is increasingly being applied to automate image interpretation, including in coronary optical coherence tomography (OCT), the gold standard for in vivo assessment of atherosclerotic plaques. Most AI models are trained using expert annotations; however, human interpretation is inherently subjective and may limit model performance. Therefore, validation against the true reference standard—histology—remains essential. The study aims to evaluate and compare the performance of an AI-powered plaque characterization model with that of clinicians, using co-registered histology as the reference standard.

Methods: Matched OCT pullbacks and serial histological sections from 25 plaques in 11 swine atherosclerotic arteries were analyzed. Precise OCT–histology co-registration was achieved using a hierarchical coarse-to-fine approach, with stent edges and anatomical landmarks as references. Plaque components (fibrous, lipidic, and calcific) were manually labeled on histology and automatically segmented on OCT by the AI model. Meanwhile, three blinded readers with different levels of OCT expertise independently annotated the corresponding frames. The relative percentages of plaque components derived from OCT were compared with histology.

Results: Across all histological sections, the median percentages of fibrous, lipidic, and calcific components were 65.0% (interquartile range [IQR]: 53.9%–92.5%), 34.3% (IQR: 6.5%–44.7%), and 0.2% (IQR: 0%–1.9%), respectively. The AI model demonstrated excellent correlation with histology, with Spearman's $\rho = 0.907$ ($P < 0.001$) for fibrous and $\rho = 0.900$ ($P < 0.001$) for lipidic components. The mean absolute discrepancy relative to histology was comparable between the AI model and the senior reader and smaller than that of the intermediate and junior readers. Agreement with histology improved with reader's experience (fibrous: intraclass correlation coefficients [ICC] = 0.666, 0.720, and 0.821; lipidic: ICC = 0.593, 0.684, and 0.803), yet remained lower than that of the AI model (fibrous: ICC = 0.938; lipidic: ICC = 0.939).

Conclusions: Despite being trained on human-annotated data, the AI model demonstrated superior agreement with histology compared with clinicians. AI-driven plaque characterization may reduce interpretative subjectivity and enhance the clinical utility of coronary OCT in the management of coronary artery disease.

Keywords: Artificial intelligence; Coronary artery disease; Histology; Optical coherence tomography

[1]*Biomedical Instrument Institute, School of Biomedical Engineering, Shanghai Jiao Tong University, Shanghai 200030, China.*[2]*Department of Cardiovascular Medicine, University of Oxford, Oxford OX3 9DU, UK.*[3]*Department of Experimental Cardiology, Erasmus Medical Center, Rotterdam 3015 GD, the Netherlands.*[4]*Cardiovascular Disease Chair, Department of Internal Medicine (Di.M.I.), University of Genoa, Genoa 16132, Italy.*[5]*Department of Chemical Engineering, Delft University of Technology, Delft 2629 HZ, the Netherlands.*[6]*Bundeswehrzentralkrankenhaus (Federal Army Central Military Hospital), Koblenz 56072, Germany.*

Miao Chu and Francesca Razzi contributed equally to this work.

**Corresponding author: Shengxian Tu, E-mail: sxtu@sjtu.edu.cn*

Cardiology Plus (2026) 11:2

Received: 12 May 2025; Accepted: 30 October 2025

http://dx.doi.org/10.1097/CP9.0000000000000158

INTRODUCTION

The buildup of atherosclerotic plaques within the vessel wall is the pathophysiological substrate underlying coronary artery disease (CAD)[1], which remains a leading cause of mortality and morbidity worldwide. Plaque characterization is of significant clinical value in aiding patient risk stratification and guiding interventional treatments[2–6]. Intravascular imaging via optical coherence tomography (OCT) allows in vivo assessment of atherosclerosis with high resolution[7], and has been validated against histology over the past decades[8]. However, manual quantification of OCT images may overburden clinicians and introduce subjectivity, especially in the catheterization laboratory setting where rapid decision-making is necessary during daily practice. This limitation hinders OCT from fully exerting its

effectiveness in CAD management[9], reinforcing the need for standardized interpretation.

To facilitate OCT assessment, many studies have been proposed automating image interpretation with the assistance of artificial intelligence (AI)[10–12]. Our group has previously developed a novel AI model using one of the largest datasets with the most comprehensive labels[13]. Notably, the model employed an innovative pseudo-3D input by feeding consecutive multi-frame image into the model, mimicking the human decision-making process in which adjacent frames are referenced during image interpretation. The model achieved high accuracy in external validation using an independent dataset from real-world clinical practise, with experts' consensus as the reference standards. Given the inevitable human subjectivity in interpreting plaque phenotypes[13], validation of the AI model against the true "gold standard" of histology remains critical yet scarce. Moreover, whether AI has the capability to recognize features and interpret images surpassing experts' ability is of considerable interest.

The objectives of the present study are to investigate the performance of the AI-empowered model for plaque characterization using co-registered histology as the gold standard and to perform a head-to-head comparison between AI and manual interpretation.

METHODS

Study design and animals

The study flowchart is shown in Figure 1. Six familial hypercholesterolemia French Bretoncelles-Meishan (FBM) minipigs, homozygous for the *LDLR R84C* mutation, were involved[14]. This genetic alteration, combined with a high-fat diet, led to the development of atherosclerosis resembling human coronary plaques. The coronary arteries included in the present analysis were derived from a previous study[15], in which drug-eluting stents were implanted and serial OCT imaging was performed before and after stenting, with an additional follow-up at 28 days.

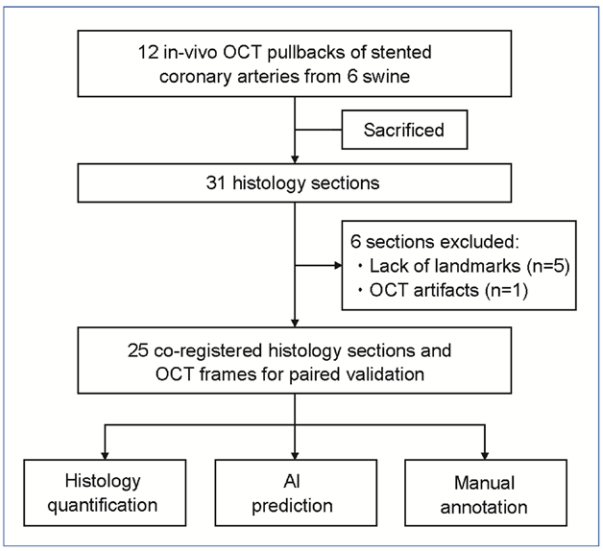

Figure 1. Study flowchart.
A total of 25 matched OCT frames and histology sections of 11 coronary arteries were included for histological validation of the AI model and for comparison with three clinicians with varying levels of OCT imaging experience.
AI: artificial intelligence; OCT: optical coherence tomography.

The diameters of the porcine coronary artery were comparable to those of humans, measuring approximately 5 mm proximally in the right coronary artery and 4 to 5 mm in the left circumflex and left anterior descending coronary arteries. As previously described[15], the animals received either a thin-strut (64 µm) cobalt-chromium sirolimus-eluting stent (SES) with an absorbable coating, 15 mm in length (n = 7; MiStent®; Micell Technologies, Inc., Durham, NC, USA), or a thin-strut (60 or 80 µm) cobalt-chromium SES, 13 mm (n = 5) or 15 mm (n = 2) in length (Orsiro®; Biotronik AG, Bülach, Switzerland). In vivo OCT imaging was performed using the Dragonfly Optis Imaging Catheter (St. Jude Medical, St. Paul, MN, USA) with a pullback speed of 36 mm/s and a frame rate of 180 frames/s. Plaque analysis was conducted on non-stented coronary segments identified from post-stent OCT pullbacks, ensuring reliable assessment of native plaque characteristics without interference from strut-induced artifacts. Afterward, the animals were sacrificed and necropsy was performed for subsequent histology analysis. The exclusion criteria included: (1) absence of a reliable match between histology and OCT due to the lack of anatomical landmarks; (2) poor image quality or the presence of image artifacts that impaired clear visualization of plaques.

The animal study protocol was approved by the Animals Ethics Committee of the Erasmus University Medical Center (the Netherlands, EMC3125 [109-12-25]). The study was conducted according to the National Institutes of Health Guide for Care and Use of Laboratory Animals and ARRIVE guidelines[16].

Histology

Upon sacrifice, the coronary arteries were dissected out, cut into 3 mm serial transverse blocks, embedded in gelatin, slowly frozen on dry ice, and stored at –80°C. The 3 mm blocks of interest located outside the stented segments were cryosectioned with a thickness of 10 µm. The tissue sections were mounted onto glass slides and separately stained with hematoxylin and eosin (H&E), Resorcin-Fuchsin (RF), and Oil-red-O (ORO) to confirm the presence of different plaque types. Finally, the stained cryosections were digitized for further analysis using a Nanozoomer 2.0HT slide scanner (Hamamatsu Photonics, Hamamatsu, Japan) at 20× magnification.

The present study used gelatin cryosections rather than formalin-fixed paraffin-embedded (FFPE) tissue to achieve better preservation and quantification of lipid composition provided by ORO staining. FFPE

processing may compromise the efficacy of ORO staining due to potential interference with lipid structures during fixation and embedding. In addition, ORO staining on paraffin sections predominantly captures the footprint of cholesterol crystals or larger droplets; consequently, smaller extracellular lipid droplets may remain undetected.

Annotation and quantification of the histology staining

An experienced histology analyst (FR), under the supervision of a trained histopathologist (HvB), annotated the digitized histological sections by outlining the contours of different plaque components (i.e., fibrous, lipidic, and calcific), with cross-confirmation using ORO, H&E, and RF staining on adjacent sections. Fibrous components within atheroma and intimal thickening were considered as a single category. Plaques without lipids or calcifications were classified as pure fibrous plaques, whereas plaques containing lipids or calcifications were classified as lipidic or calcified plaques, respectively. The percentage of each plaque component was calculated as the ratio of the summed pixel numbers of that component to the total number of pixel amid the lumen contour and the internal elastic lamina (IEL). Histological annotations were performed blinded to the OCT results.

Co-registration of OCT image and histology

Co-registration of histological sections with the corresponding OCT frames was performed through a coarse-to-fine strategy, with stent edge and anatomical landmarks serving as references. First, the index OCT frame was determined according to the longitudinal distance from the stent edge. Subsequently, seven adjacent frames both proximally and distally to the index frame were reviewed, resulting in an approximately 3 mm OCT segment of interest, comparable to the length of the arterial block. Finally, the optimal matching OCT frame within the segment was selected according to the anatomical landmarks, including side branches, arterial and plaque morphology, and the presence of specific plaque components (i.e., lipid and calcification).

OCT analysis and plaque characterization by the AI model

The OCT images were analyzed at an independent core laboratory (CardHemo, Med-X Research Institute, Shanghai Jiao Tong University) by an experienced analyst (M.Chu) using a commercially available software program (OctPlus, version V2; Pulse Medical, Shanghai, China). The OCT images were automatically segmented by the AI model embedded in the software, which has been previously described and validated[13]. Briefly, a novel convolutional neural network was developed using a large dataset of over 10,000 frames. Consecutive OCT frames were fed into the AI model as pseudo-3D input, emulating clinicians who consider adjacent images when interpreting images. The developed AI model enabled automatic delineation of different plaque components amid the lumen and IEL, including fibrous, lipidic, and calcific components. Quantitative parameters such as plaque percentages were automatically derived by the software based on the AI outputs.

Manual annotation on OCT

Three interventional clinicians with <1, around 2, and >10 years of OCT clinical experience, who have interpreted approximately 100, 300, and >1,000 OCT images, respectively, were referred to as junior, intermediate, and senior readers. They annotated the OCT frames blinded to both histology and AI predictions. First, lumen and IEL contours were delineated, followed by labeling of different plaque components (i.e., fibrous, lipidic, and calcific) on the target OCT frame with references to adjacent segments. The proportion of each plaque component was calculated using the same method applied in histology.

Statistical analysis

Continuous variables are reported as mean ± standard deviation (SD) or as median and interquartile range (IQR), as appropriate. Normal distribution of continuous variables was tested using the Shapiro-Wilk test. The correlation and agreement between OCT-derived and histology-derived plaque percentages were evaluated using Spearman's rank correlation coefficient (ρ), intraclass correlation coefficient (ICC), and Bland–Altman plots. To assess potential clustering of sections within arteries, a null-model multilevel analysis was performed to estimate the arterial-level effect.

Regression modeling was implemented to investigate the relationships between AI-derived and histology-derived continuous variables, denoted by the coefficient of determination (R^2). To ensure robust estimation of the regression parameters, bias-corrected 95% confidence intervals (95% CIs) for the slope and intercept were constructed using a bootstrap analysis. Specifically, the bootstrap procedure involved 500 iterations of sampling with replacement from the original dataset to estimate the variability and distribution of these parameters.

All statistical analyses were performed with SPSS version 20.0 (SPSS Inc., Chicago, IL, USA). P values were two-sided and considered statistically significant if <0.05.

RESULTS

A total of 31 histology sections from 12 coronary arteries of six atherosclerotic swine were initially enrolled

and 25 matched OCT frames and histology sections from 11 arteries were included in the final analysis (Figure 1). Six histology sections were excluded due to the absence of matched anatomical landmarks (n = 5) and OCT image artifacts (n = 1). Figure 2 shows two representative examples of co-registration and plaque characterization between matched histology staining and OCT images.

Histology quantification

Histological analysis showed that the involved arteries presented a variety of plaque types, varying from purely fibrous to lipid-rich plaques. Two out of 25 sections (8%) were purely fibrous, whereas lipidic and calcific components were present alongside fibrous components in 21 sections (84%) and 15 sections (60%), respectively. Fibrous, lipidic, and calcific components accounted for 65.0% (IQR: 53.9%–92.5%), 34.3% (IQR: 6.5%–44.7%), and 0.2% (IQR: 0%–1.9%) of the total plaque components across all sections (Figure 3).

OCT plaque characterization

Figure 3 shows the distributions of different plaque components on OCT derived by manual annotation and the AI model. The median percentages for fibrous and lipidic components derived from the AI model were 68.6% (IQR: 57.5%–100%) and 31.4% (IQR: 0%–42.5%), respectively. Two slices contained small calcific components identified by the AI model, with percentages of 2.1% and 5.3%, whereas the corresponding histology showed 1.8% and 7.0%, respectively.

Large deviations in plaque percentages were observed among manual annotations. The median values for fibrous components were 100% (IQR: 57.9%–100%), 48.5% (IQR: 31.3%–72.9%), and 86.7% (IQR: 49.1%–100%), while the median values for lipidic components were 0% (IQR: 0%–38.2%), 51.5% (IQR: 27.1%–68.7%), and 13.3% (0%–51.0%), for the junior, intermediate, and senior readers, respectively. Calcific components were not identified in any OCT frame by the intermediate or senior readers. However, the junior analyst labeled and overestimated calcific components in two OCT frames with percentages of 13.6% and 18.3%, where the corresponding histology showed calcific percentages of 1.8% and 0.5%, respectively.

Agreement between AI-OCT and histology

Excellent correlations were observed between AI-derived and histology-derived plaque percentages, with Spearman coefficients of $\rho = 0.907$ (95% CI: 0.786–0.956; $P < 0.001$) for fibrous components and $\rho = 0.900$ (95% CI: 0.771–0.953; $P < 0.001$) for lipidic components (Figure 4A and 4B).

Bland–Altman analysis indicated good agreement between the AI model and histology, with ICC of 0.938 (95% CI: 0.841–0.974) for fibrous components and 0.939 (95% CI: 0.861–0.973) for lipidic components (Figure 4C and 4D). Linear regression modeling demonstrated significant relationships between AI-OCT and histology-derived plaque percentages, with slopes and intercepts shown in Table 1. Multilevel model analysis

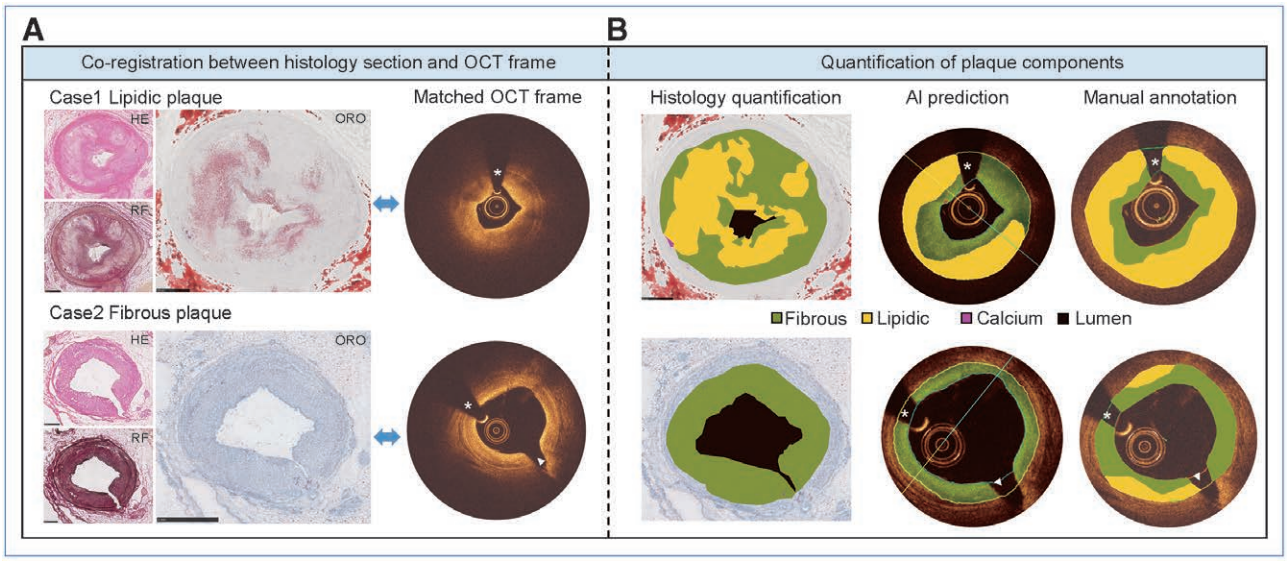

Figure 2. Representative examples of matched histology and OCT for lipidic and fibrous plaques.
A. Co-registration between the histology section and OCT frame was performed according to the longitudinal distance to stent edge, anatomical markers of side branches, and plaque morphology; **B.** Plaque quantification was performed on histology and on OCT by the AI model and clinicians, with the annotations overlaid on the ORO and OCT images, respectively. The shape of plaque components may be different between OCT and histology due to tissue deformation in the histological staining. Side branch and guidewire artifacts on OCT are indicated with an arrowhead and asterisk, respectively.
AI: artificial Intelligence; HE: hematoxylin and eosin; OCT: optical coherence tomography; ORO: Oil-red-O; RF: Resorcin-Fuchsin.

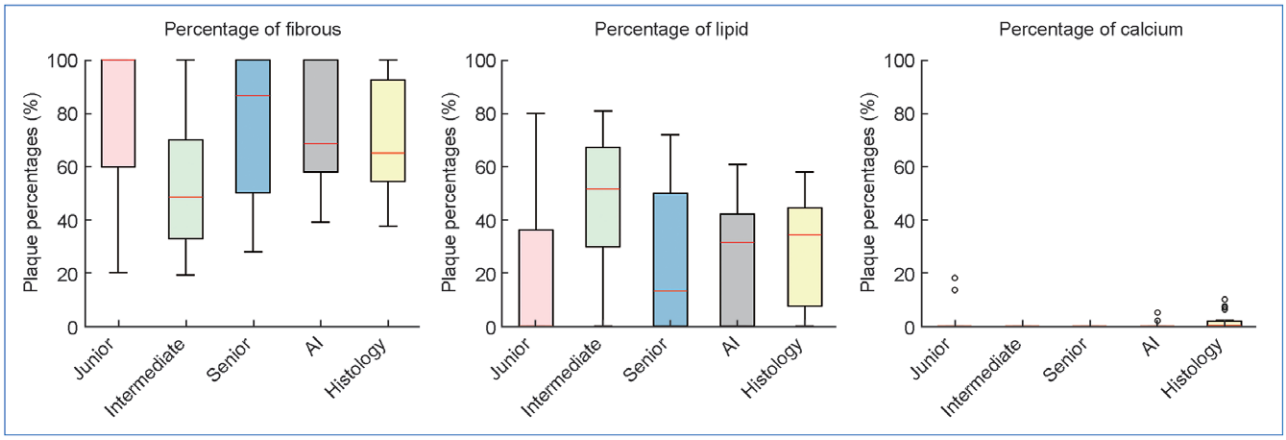

Figure 3. Comparison of plaque percentages derived from OCT and histology.
Manual annotations exhibited high inter-reader variability, with large deviations in plaque percentages across analysts.
AI: artificial intelligence; OCT: optical coherence tomography.

excluded a potential clustering effect at the arterial level (P = 0.111). The outliers shown in Figure 4 were mainly caused by the underestimation of lipidic plaque and undetected small calcification.

Comparison between human readers and AI

Agreement with histology improved as the reader's level of expertise increased, as shown in Table 2. The AI model showed superior agreement with histology compared with all readers. The mean discrepancy in plaque percentage relative to histology was similar between the AI and the senior reader, and smaller than that observed for the junior and intermediate readers. Compared with histology, both the AI model and the senior reader tended to overestimate fibrous components and underestimate lipidic components (Table 2). Notably, the AI model displayed smaller SDs than all readers, indicating better consistency in measurements.

DISCUSSION

For the first time, the performance of AI-empowered automatic plaque characterization on coronary OCT images was compared with human-based interpretation in a head-to-head way, using histology as the gold standard. The AI model, trained on human annotations, showed high agreement with histology and demonstrated the potential to surpass the image interpretation skills of some inexperienced clinicians. Meanwhile, clinicians' diagnostic performance in plaque characterization improved as their OCT expertise increased.

The characterization of coronary plaque features has significant prognostic and therapeutic implications. Multiple studies have demonstrated that specific plaque morphologies, such as high plaque burden, large lipid cores, thin fibrous caps, and calcification, are associated with an increased risk of adverse cardiovascular events. For example, the PROSPECT II Trial[6] identified large plaque burden and highly lipidic lesions as independent predictors of future events, while the CLIMA[2] and COMBINE OCT-FFR[4] studies further emphasized the role of high-risk features such as thin-cap fibroatheroma (TCFA) and macrophage infiltration in predicting plaque vulnerability.

Thanks to its superior spatial resolution, OCT imaging offers advantages over intravascular ultrasound (IVUS) in assessing fibrous cap, features of plaque vulnerability, and calcifications[17–18]. Although evidence has demonstrated favorable clinical outcomes with OCT-guided interventions in different scenarios[19–21], the adoption of OCT in routine clinical practice has been partly limited by the subjectivity and variability of image interpretation[9,22]. For example, in the COMBINE OCT-FFR Trial[4], the inter-rater agreement for OCT-defined TCFA was $\kappa = 0.81$ (95% CI: 0.70–0.97), and intra-rater agreement was $\kappa = 0.78$ (95% CI: 0.61–0.92). This highlights a pressing need for tools that can standardize and streamline OCT interpretation.

AI-driven analysis of OCT offers a promising pathway to enhance the clinical utility of plaque characterization. By enabling automated, real-time identification of plaque components, AI can support decision-making during OCT-guided PCI and reduce the dependency on expert interpretation. This is particularly relevant in the context of large-scale imaging trials such as ILUMIEN[21] and Optical Coherence Tomography Optimized Bifurcation Event Reduction (OCTOBER)[3], which aim to assess the impact of OCT-guided PCI on clinical outcomes. In such trials, real-time AI support could facilitate consistent and efficient interpretation of plaque morphology, guide stent sizing and implantation, and help identify high-risk plaques that may benefit from intensified medical therapy or closer follow-up. As AI tools continue to mature, they may play a key role in scaling the adoption of OCT-guided interventions.

While AI has been applied to provide automated OCT interpretation in recent years[11–12,23–24], the majority of

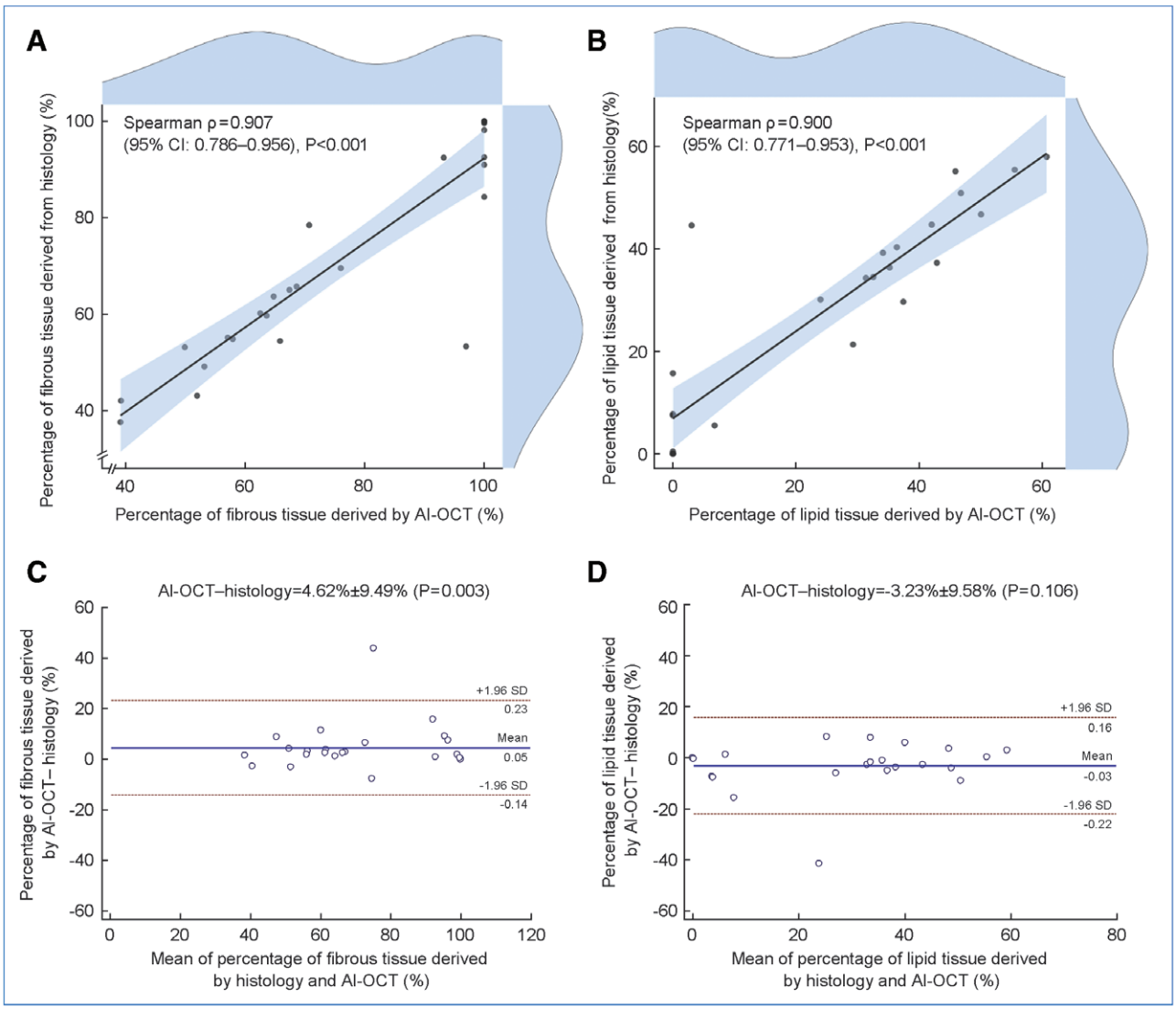

Figure 4. Agreement between AI predictions and histology in quantifying plaque components.
A–B, Correlations for the percentages of fibrous and lipidic tissue derived from AI and histology with linear regression modeling and its CI. The slope and intercept by the mixed linear regression are detailed in Table 2. Marginal density distributions (blue shading) along the top and right axes reflect sample clustering patterns; **C–D,** Bland–Altman plots. Middle blue line: mean difference; red dotted lines: mean ± 1.96 SD.
95% CI: 95% confidence interval; AI: artificial Intelligence; OCT: optical coherence tomography; SD: standard deviation.

Table 1.
Mixed linear regression analysis of AI-OCT–derived and histology-derived plaque percentages

	Slope	P value	Intercept	P value	R^2
Percentage of fibrous	0.875 (0.689–1.061)	<0.001	0.049 (–0.094 to 0.192)	0.484	0.813
Percentage of lipid	0.851 (0.667–1.035)	<0.001	0.069 (0.010–0.128)	0.025	0.799

Bias-corrected 95% CI from a bootstrap analysis are reported for slope and intercept, with the pullback as cluster and performed 500 replications.
95% CI: 95% confidence interval; AI: artificial intelligence; OCT: optical coherence tomography.

studies have relied solely on expert-derived OCT annotations for both model development and validation. A small number of studies have attempted to incorporate histology-based labeling[25–26], but these efforts have typically been constrained by very limited sample sizes for developing robust models[27]. In contrast, our AI model was developed based on a large, diverse multicenter dataset of over 10,000 expert-annotated OCT frames[13], and was subsequently validated against histology as the true reference standard in the present study.

To address the penetration limitation inherent to OCT[7], our AI model was developed by inputting consecutive OCT frames rather than a single cross-section, together with a priori knowledge of spatial continuity. This strategy enabled the model to generate reliable extrapolations for deep atheroma with signal

Table 2.
Discrepancies between OCT-derived and histology-derived plaque percentages

	ICC	OCT–histology	P value
Percentage of fibrous			
Junior	0.666 (0.246–0.846)	8.52% ± 23.03%	0.130
Intermediate	0.720 (0.021–0.900)	–17.34% ± 17.88%	<0.001
Senior	0.821 (0.598–0.921)	4.01% ± 18.88%	0.316
AI model	0.938 (0.841–0.974)	4.62% ± 9.49%	0.003
Percentage of lipid			
Junior	0.593 (0.113–0.817)	–8.12% ± 24.21%	0.115
Intermediate	0.684 (–0.076 to 0.888)	19.02% ± 18.16%	<0.001
Senior	0.803 (0.552–0.913)	–2.33% ± 19.56%	0.614
AI model	0.939 (0.861–0.973)	–3.23% ± 9.58%	0.106

Data are presented as ICC with 95% CI and mean ± SD for the percentage difference of plaque between OCT measurements (manual by physicians of different seniority and AI model) and histology. 95% CI: 95% confidence interval; AI: artificial intelligence; ICC: intraclass correlation coefficient; OCT: optical coherence tomography; SD: standard deviation.

attenuation. Consequently, the AI model showed good performance in plaque burden assessment not only compared with manual OCT analysis but also with co-registered IVUS images[28]. In line with these findings, the present study demonstrated satisfactory concordance between the percentage of lipidic components derived by the AI model and those derived from histology (AI – histology = –3.23% ± 9.58%). The outliers observed in Figure 4 were mainly caused by the underestimation of lipidic plaques and undetected calcifications.

Although atherosclerotic swine models are not identical to humans, studies have suggested that pigs with familial hypercholesterolemia develop complex coronary atheroma resembling human plaques[29–30]. Notably, unlike the calcified arteries often encountered in patients, the calcific components in the animal model used in this study consisted mostly of micro-calcifications, accounting for only a very small proportion of the whole atheroma (0.23% [IQR: 0%–1.94%]). In addition, these calcific spots were mostly located beneath lipidic tissue, which precluded adequate visualization of the calcific regions. Therefore, in the current study, neither the analysts nor the AI model was able to identify the majority of calcific components.

The study involved clinicians with different levels of OCT expertise to reflect routine clinical practice. Interestingly, improved agreement with histology was observed as OCT experience increased, which reflected the importance of adequate training. The good concordance between the AI model and histology indicates that AI may facilitate the training process for clinical trainees by providing accurate imaging interpretation. Moreover, the average analysis speed of the AI model is only a few seconds per image pullback, whereas the analysts required several hours to finish all annotations.

Limitations

Several limitations of the current study should be acknowledged. First, the AI model was developed using human-derived OCT training data but validated on a familial hypercholesterolemia swine model. Although the animal model exhibited prominent atherosclerotic features, including substantial lipid accumulation and notable plaque burden, it still had limitations in terms of the scarcity of advanced plaques, such as severely calcified plaque and TCFAs. This may have favored AI performance. Furthermore, the AI's performance in detecting cholesterol crystals or macrophages was modest and was not compared with histology. Therefore, the capability of the AI model to diagnose these phenotypes requires further validation. Future post-mortem studies using human data are needed to provide better perspectives in this regard.

Second, discrepancies existed in some morphological parameters between histology and OCT, such as plaque burden or plaque arc. These differences may have arisen from ex vivo plaque tissue deformation and distortion caused by the absence of blood pressure and the cryosectioning process. Therefore, the present study focused on calculating and comparing the proportions of different tissue components. In addition, Von Kossa staining was not available for quantifying calcification.

Third, the sample size of the study was relatively small. However, a significant trend was observed in the results, which showed statistical power. Finally, the classification of readers into senior, intermediate, and junior levels was based on clinical experience. While this approach is consistent with conventions in clinical research, it may introduce variability in defining expertise levels, particularly for intermediate readers.

CONCLUSIONS

The AI model developed for automatic plaque characterization of OCT shows good agreement with histology in external histology validation. Manual assessment of plaque characterization by clinicians improved with increasing imaging expertise. This study highlights that

the AI model has the potential to surpass human interpretation skills, thereby mitigating subjectivity in image interpretation and assisting in the training of clinical trainees.

FUNDING

This work was supported by the Natural Science Foundation of China (No. 82302285 to MC and No. 82327808 to SXT), and ZonMW, the Netherlands (grant number 114021510 to HvB and VvS).

AUTHOR CONTRIBUTIONS

MC and FR participated in the research design, data analysis, and writing of the paper. GLDM, SB, JC, WY, and RBD participated in data analysis. AB, VvS, JLGC, SXT, and HvB participated in the research design and review of the paper.

CONFLICT OF INTEREST STATEMENT

ST reported research grants and consultancy from Pulse Medical. All other authors have reported that they have no relationships relevant to the contents of this paper to disclose.

ACKNOWLEDGMENT

We would like to acknowledge the excellent support of Karin Witberg and Jurgen Ligthart for the acquisition of the OCT images, and Mathijs Stam for histology.

DATA SHARING STATEMENT

Data is available from the corresponding or senior authors upon reasonable request.

REFERENCES

[1] Koskinas KC, Ughi GJ, Windecker S, *et al*. Intracoronary imaging of coronary atherosclerosis: validation for diagnosis, prognosis and treatment. Eur Heart J 2016;37(6):524–535. doi:10.1093/eurheartj/ehv642.

[2] Prati F, Romagnoli E, Gatto L, *et al*. Relationship between coronary plaque morphology of the left anterior descending artery and 12 months clinical outcome: the CLIMA study. Eur Heart J 2020;41(3):383–391. doi:10.1093/eurheartj/ehz520.

[3] Holm NR, Andreasen LN, Neghabat O, *et al*; OCTOBER Trial Group. OCT or angiography guidance for PCI in complex bifurcation lesions. N Engl J Med 2023;389(16):1477–1487. doi:10.1056/NEJMoa2307770.

[4] Kedhi E, Berta B, Roleder T, *et al*. Thin-cap fibroatheroma predicts clinical events in diabetic patients with normal fractional flow reserve: the COMBINE OCT-FFR trial. Eur Heart J 2021;42(45):4671–4679. doi:10.1093/eurheartj/ehab433.

[5] Waksman R, Di Mario C, Torguson R, *et al*; LRP Investigators. Identification of patients and plaques vulnerable to future coronary events with near-infrared spectroscopy intravascular ultrasound imaging: a prospective, cohort study. Lancet 2019;394(10209):1618. doi:10.1016/S0140-6736(19)32276-7.

[6] Erlinge D, Maehara A, Ben-Yehuda O, *et al*. Identification of vulnerable plaques and patients by intracoronary near-infrared spectroscopy and ultrasound (PROSPECT II): a prospective natural history study. Lancet 2021;397(10278):985–995. doi:10.1016/s0140-6736(21)00249-x.

[7] Gutiérrez-Chico JL, Alegría-Barrero E, Teijeiro-Mestre R, *et al*. Optical coherence tomography: from research to practice. Eur Heart J Cardiovasc Imaging 2012;13(5):370–384. doi:10.1093/ehjci/jes025.

[8] Yabushita H, Bouma BE, Houser SL, *et al*. Characterization of human atherosclerosis by optical coherence tomography. Circulation 2002;106(13):1640–1645. doi:10.1161/01.cir.0000029927.92825.f6.

[9] Johnson T, O'Kane P. Can machine learned algorithms further illuminate intracoronary imaging in PCI and improve the human touch? AI-guided image interpretation. EuroIntervention 2021;17(1):18–19. doi:10.4244/eijv17i1a3.

[10] Abdolmanafi A, Duong L, Dahdah N, *et al*. Deep feature learning for automatic tissue classification of coronary artery using optical coherence tomography. Biomed Opt Express 2017;8(2):1203–1220. doi:10.1364/BOE.8.001203.

[11] Park S, Araki M, Nakajima A, *et al*. Enhanced diagnosis of plaque erosion by deep learning in patients with acute coronary syndromes. J Am Coll Cardiol Intv 2022;15(20):2020–2031. doi:10.1016/j.jcin.2022.08.040.

[12] Katagiri Y, Hosoi Y, Bota H, *et al*. Artificial intelligence vs visual assessment of calcified plaque in coronary artery using optical coherence tomography. JACC Adv 2022;1(4):100080. doi:10.1016/j.jacadv.2022.100080.

[13] Chu M, Jia H, Gutierrez-Chico JL, *et al*. Artificial intelligence and optical coherence tomography for the automatic characterisation of human atherosclerotic plaques. EuroIntervention 2021;17(1):41–50. doi:10.4244/EIJ-D-20-01355.

[14] Hoogendoorn A, den Hoedt S, Hartman EM, *et al*. Variation in coronary atherosclerosis severity related to a distinct LDL (low-density lipoprotein) profile. ATVB 2019;39(11):2338–2352. doi:10.1161/atvbaha.119.313246.

[15] Razzi F, Dijkstra J, Hoogendoorn A, *et al*. Plaque burden is associated with minimal intimal coverage following drug-eluting stent implantation in an adult familial hypercholesterolemia swine model. Sci Rep 2023;13(1):10683. doi:10.1038/s41598-023-37690-0.

[16] Kilkenny C, Browne W, Cuthill IC, *et al*; NC3Rs Reporting Guidelines Working Group. Animal research: reporting in vivo experiments: the ARRIVE guidelines. Br J Pharmacol 2010;160(7):1577–1579. doi:10.1111/j.1476-5381.2010.00872.x.

[17] Mintz GS. Intravascular imaging of coronary calcification and its clinical implications. JACC Cardiovasc Imaging 2015;8(4):461–471. doi:10.1016/j.jcmg.2015.02.003.

[18] van Soest G, Marcu L, Bouma BE, *et al*. Intravascular imaging for characterization of coronary atherosclerosis. Curr Opin Biomed Eng 2017;3:1–12. doi:10.1016/j.cobme.2017.07.001.

[19] Lee JM, Choi KH, Song YB, *et al*; RENOVATE-COMPLEX-PCI Investigators. Intravascular imaging-guided or angiography-guided complex PCI. N Engl J Med 2023;388(18):1668–1679. doi:10.1056/NEJMoa2216607.

[20] Hong SJ, Kim BK, Shin DH, *et al*; IVUS-XPL Investigators. Effect of intravascular ultrasound-guided vs angiography-guided everolimus-eluting stent implantation: the IVUS-XPL randomized clinical trial. JAMA 2015;314(20):2155–2163. doi:10.1001/jama.2015.15454.

[21] Ali ZA, Maehara A, Généreux P, *et al*; ILUMIEN III: OPTIMIZE PCI Investigators. Optical coherence tomography compared with intravascular ultrasound and with angiography to guide coronary stent implantation (ILUMIEN III: OPTIMIZE PCI): a randomised controlled trial. Lancet 2016;388(10060):2618–2628. doi:10.1016/S0140-6736(16)31922-5.

[22] Koskinas KC, Nakamura M, Räber L, *et al*. Current use of intracoronary imaging in interventional practice—results of a European Association of Percutaneous Cardiovascular Interventions (EAPCI) and Japanese Association of Cardiovascular Interventions and Therapeutics (CVIT) clinical practice survey. EuroIntervention 2018;14(4):e475–e484. doi:10.4244/EIJY18M03_01.

[23] Abdolmanafi A, Duong L, Ibrahim R, *et al*. A deep learning-based model for characterization of atherosclerotic plaque in coronary arteries using optical coherence tomography images. Med Phys 2021;48(7):3511–3524. doi:10.1002/mp.14909.

[24] Lee J, Gharaibeh Y, Kolluru C, *et al*. Segmentation of coronary calcified plaque in intravascular OCT images using a two-step

deep learning approach. IEEE Access 2020;8:225581–225593. doi:10.1109/access.2020.3045285.
[25] He CL, Li ZL, Wang JQ, *et al*. Atherosclerotic plaque tissue characterization: an OCT-based machine learning algorithm with ex vivo validation. Front Bioeng Biotechnol 2020;8:749. doi:10.3389/fbioe.2020.00749.
[26] Baruah V, Zahedivash A, Hoyt T, *et al*. Automated coronary plaque characterization with intravascular optical coherence tomography and smart-algorithm approach: virtual histology OCT. JACC Cardiovasc Imaging 2020;13(8):1848–1850. doi:10.1016/j.jcmg.2020.02.022.
[27] Chu M, Wu P, Li G, *et al*. Advances in diagnosis, therapy, and prognosis of coronary artery disease powered by deep learning algorithms. JACC Asia 2023;3(1):1–14. doi:10.1016/j.jacasi.2022.12.005.
[28] Sukhanov S, Higashi Y, Yoshida T, *et al*. Insulin-like growth factor 1 reduces coronary atherosclerosis in pigs with familial hypercholesterolemia. JCI Insight 2023;8(4):e165713. doi:10.1172/jci.insight.165713.
[29] Thim T, Hagensen MK, Drouet L, *et al*. Familial hypercholesterolaemic downsized pig with human-like coronary atherosclerosis: a model for preclinical studies. EuroIntervention 2010;6(2):261–268. doi:10.4244/EIJV6I2A42.
[30] Huang JY, Tu SX, Masuda S, *et al*. Plaque burden estimated from optical coherence tomography with deep learning: in vivo validation using co-registered intravascular ultrasound. Catheter Cardiovasc Interv 2023;101(2):287–296. doi:10.1002/ccd.30525.

How to cite this article: Chu M, Razzi F, De Maria GL, Benenati S, Chai J, Yu W, Dai RB, van Steijn V, Banning A, Gutiérrez-Chico JL, Tu SX, van Beusekom H. Histological validation of artificial intelligence–driven automatic plaque characterization in coronary OCT: a head-to-head comparison with clinicians. Cardiol Plus 2026;00:00–00. doi: 10.1097/CP9.0000000000000158.